Cellular/Molecular

T-Type Ca²⁺ Channels Mediate a Critical Period of Plasticity in Adult-Born Granule Cells

William M. Kennedy, Jose Carlos Gonzalez, Haeun Lee, Jacques I. Wadiche, and Linda Overstreet-Wadiche

Department of Neurobiology and McKnight Brain Institute, University of Alabama at Birmingham, Birmingham, Alabama 35294

Adult-born granule cells (abGCs) exhibit a transient period of elevated synaptic plasticity that plays an important role in hippocampal function. Various mechanisms have been implicated in this critical period for enhanced plasticity, including minimal GABAergic inhibition and high intrinsic excitability conferred by T-type Ca²⁺ channels. Here we assess the contribution of synaptic inhibition and intrinsic excitability to long-term potentiation (LTP) in abGCs of adult male and female mice using perforated patch recordings. We show that the timing of critical period plasticity is unaffected by intact GABAergic inhibition such that 4–6-week-old abGCs exhibit LTP that is absent by 8 weeks. Blocking GABA$_A$ receptors, or partial blockade of GABA release from PV and nNos-expressing interneurons by a μ-opioid receptor agonist, strongly enhances LTP in 4-week-old GCs, suggesting that minimal inhibition does not underlie critical period plasticity. Instead, the closure of the critical period coincides with a reduction in the contribution of T-type Ca²⁺ channels to intrinsic excitability, and a selective T-type Ca²⁺ channel antagonist prevents LTP in 4-week-old but not mature GCs. Interestingly, whole-cell recordings that facilitate T-type Ca²⁺ channel activity in mature GCs unmasks LTP (with inhibition intact) that is also sensitive to a T-type Ca²⁺ channel antagonist, suggesting T-type channel activity in mature GCs is suppressed by native intracellular signaling. Together these results show that abGCs use T-type Ca²⁺ channels to overcome inhibition, providing new insight into how high intrinsic excitability provides young abGCs a competitive advantage for experience-dependent synaptic plasticity.

Key words: adult neurogenesis; dentate gyrus; excitability; inhibition; LTP; opioid

Significance Statement

Adult-born granule cells (abGCs) exhibit a transient period of elevated synaptic plasticity that is thought to play an important role in hippocampal function. Here we address the cellular mechanisms that underlie this "critical period" for plasticity. We show that the closure of the critical period corresponds with loss of intrinsic excitability mediated by T-type Ca²⁺ channels and that T-type Ca²⁺ channels promote long-term synaptic plasticity in abGCs despite strong GABA$_A$ receptor-mediated inhibition. Regulation of Ca²⁺ channel function contributes to the loss of excitability and LTP mediated by T-type Ca²⁺ channels in mature GCs. These results provide insight into how intrinsic excitability and inhibition contribute to plasticity in the dentate gyrus.

Introduction

The dentate gyrus continually produces new excitatory granule cells (GCs) throughout life. There is ample evidence that some

hippocampal-dependent behaviors correlate with the extent of neurogenesis and the magnitude of long-term synaptic potentiation (LTP) in the dentate gyrus, leading to the idea that neurogenesis provides an essential substrate for experience-dependent plasticity. For example, selective manipulations of young adult-born GCs (abGCs) alter performance of contextual discrimination tasks that develop over multiple trials and also alter dentate gyrus LTP (Clelland et al., 2009; Deng et al., 2009; Massa et al., 2011; Sahay et al., 2011; Kheirbek et al., 2012; Nakashiba et al., 2012). Recordings from individual abGCs confirm a high propensity for LTP from 4 to 6 weeks after cell birth that subsequently declines by 8 weeks (Schmidt-Hieber et al., 2004; Ge et al., 2007). The transient period of high synaptic plasticity, often called a "critical period," strongly influences ideas about the role of continual neurogenesis in experience-

dependent circuit modification and memory function (Schinder and Gage, 2004; Miller and Sahay, 2019; Cushman et al., 2021), yet the cellular mechanisms underlying this plasticity are unclear.

One long-standing idea is that young abGCs are insensitive to synaptic inhibition that restricts plasticity in mature GCs (Wang et al., 2000; Snyder et al., 2001), akin to the role of inhibition controlling the critical period of ocular dominance plasticity (Fagiolini and Hensch, 2000). In the first weeks after cell birth, GABA$_A$ receptor-mediated depolarization drives dendrite growth and synapse formation by AMPAR insertion and in some conditions, action potentials (Ge et al., 2006; Chancey et al., 2013; Heigele et al., 2016). The chloride equilibrium potential (E_{Cl}) that determines the polarity of GABA$_A$ receptor-mediated potentials reaches mature values by the 4th week after abGC birth (Ge et al., 2006). Yet 4-week-old (4w) abGCs exhibit less GABAergic synaptic connectivity compared with neighboring mature GCs, supporting the notion that abGCs are less inhibited than mature GCs (Li et al., 2012; Marin-Burgin et al., 2012; Dieni et al., 2013; Temprana et al., 2015; Groisman et al., 2020). In fact, results using field potential recordings show that LTP in control conditions (i.e., ACSF-LTP) originates primarily from the small population of young abGCs, while LTP in the presence of GABA$_A$ receptor antagonists reflects plasticity in the large population of mature GCs (Snyder et al., 2001; Saxe et al., 2006; Massa et al., 2011; Mongiat and Schinder, 2011).

Whether the development of inhibitory circuitry underlies the closing of the critical period for plasticity in abGCs has not been explicitly tested. But single-cell recordings have revealed properties of abGCs that promote LTP when synaptic inhibition is blocked, suggesting additional mechanisms for critical period plasticity. For example, young abGCs exhibit T-type Ca^{2+} spikes that boost intrinsic excitability, predicting that T-type channels reduce the threshold for LTP via a global rise in Ca^{2+} and/or relief of voltage-dependent Mg^{2+} block (Schmidt-Hieber et al., 2004). Young abGCs also have a large NMDAR:AMPAR ratio and NR2B subunit-containing NMDARs associated with highly plastic immature synapses (Tovar and Westbrook, 1999; Ge et al., 2007; Kheirbek et al., 2012; Chancey et al., 2013; Schmidt-Salzmann et al., 2014; Dieni et al., 2016; Li et al., 2017). Nonetheless, dendritic depolarization and NMDAR activation essential for LTP induction are controlled by GABAergic inhibition (Schulz et al., 2018). Although abGCs exhibit delayed innervation from proximal projecting PV- and SST-expressing interneurons (Groisman et al., 2020; Remmers et al., 2020), by 1–2 weeks of age (newborn) abGCs exhibit GABA$_A$ receptor-mediated currents from dendritic-projecting interneurons like ivy/neurogliaform cells, with functional inhibition evident by 4 weeks after cell birth (Markwardt et al., 2011; Dieni et al., 2013; Vaden et al., 2020). Here, we investigate how inhibition and intrinsic excitability contribute to LTP in abGCs during the critical period. We find that inhibition does not alter the timing of the critical period and strongly suppresses LTP in 4w abGCs, ruling out an essential contribution of interneuron circuit development for critical period plasticity. Conversely, our results suggest that changes in intrinsic excitability and T-type Ca^{2+} channel function contribute to the closing of the critical period.

Materials and Methods

All animal procedures followed the Guide for the Care and Use of Laboratory Animals, U.S. Public Health Service, and were approved by the University of Alabama at Birmingham Institutional Animal Care. Male and female mice 2–4 months of age were used for experiments.

Mice were maintained in standard housing on a 12 h light/dark cycle with *ad libitum* access to food and water, with experiments performed during the light phase. Mouse lines used to generate experimental mice included *Ascl1^{CreERT2}* (Jax# 012882), *Ai14* (Jax# 7914), and wildtype C57BL/6J (Jax# 664). A few datasets included mature GCs recorded in slices from *nNOS-CreER* (Taniguchi et al., 2011; Jax# 014541) or *PV^{Cre}* (Jax# 017320) mice crossed with *Ai32* mice (Jax# 24109). nNOS-Cre^{ER} mice were fed tamoxifen-containing chow (Teklad250) for 4 d at weaning. *Ascl1^{CreERT2}* mice were injected with tamoxifen (tmx 0.12 mg/g, dissolved in 10% EtOH/90% sunflower oil) intraperitoneally once a day for 2 d at 6 weeks of age (Yang et al., 2015). Standard Jackson Laboratory protocols for genotyping were used to identify Cre$^+$ tdT$^+$ offspring used in experiments.

Morphology. Mice were anesthetized by inhalation of isoflurane and deeply anesthetized with subsequent intraperitoneal injection of 2,2,2-tribromoethanol (Avertin; Sigma-Aldrich). Anesthetized mice were perfused intracardially with 0.1 M PBS and chilled 4% PFA before brains were removed and postfixed overnight in PFA. Free-floating horizontal slices were made on a Vibratome 1000 (50 μm). Slices were mounted with ProLong Gold or VectaShield mounting medium (Invitrogen). Slices were imaged on an Olympus FluoView 1200 confocal microscope with a 20× objective using a z-step of 5 μm. For cell reconstructions, abGCs were imaged with a 40× objective using a step size of 1 μm. An investigator blinded to the cell ages analyzed dendritic morphology using Neurolucida (MicroBrightField). Measurements and analysis of total dendrite length (TDL) and Sholl analysis of length and intersections were performed using Neurolucida Explorer.

Electrophysiology. Mice were lightly anesthetized by inhalation of isoflurane and deeply anesthetized with an intraperitoneal injection of 2,2,2-tribromoethanol (Avertin; Sigma-Aldrich). Mice were then intracardially perfused with ice-cold cutting solution containing the following (in mM): 110 choline chloride, 25 glucose, 7 MgCl$_2$, 2.5 KCl, 1.25 Na$_2$PO$_4$, 0.5 CaCl$_2$, 1.3 Na-ascorbate, 3 Na-pyruvate, and 25 NaHCO$_3$, bubbled with 95% O$_2$/5% CO$_2$. The brain was quickly removed and 300 μm horizontal slices were prepared using a vibratome (Leica VT1200S; Bischofberger et al., 2006). Slices were incubated at 37°C for 30 min in recording solution (ACSF) containing the following (in mM): 125 NaCl, 2.5 KCl, 1.25 Na$_2$PO$_4$, 2 CaCl$_2$, 1 MgCl$_2$, 25 NaHCO$_3$, and 25 glucose bubbled with 95% O$_2$/5% CO$_2$ before transfer to room temperature for at least 30 min before recording. Experiments were performed at 30 ± 2°C.

Pipettes were pulled from thick-walled borosilicate glass with filament (1.5/0.86 mm; #BF150-86-10; Sutter). Perforated patch recordings used a pipette solution containing the following (in mM): 140 KCl, 4 MgCl$_2$, 10 EGTA, 10 HEPES, pH 7.3 (312 mOsm, 3–6 MΩ). A stock of gramicidin A-containing solution was prepared every 1–4 d (10 mg/ml in DMSO; G5002; Sigma Life Sciences). The stock solution was vortexed and sonicated for 10–15 min and then diluted in the pipette solution to achieve a final working concentration (10–100 μg/ml). The gramicidin pipette solution was vortexed (∼10 s) and then sonicated for an additional 5–10 min before use. Pipettes were backfilled to half the taper with gramicidin-free solution to prevent gramicidin from interfering with seal formation. Current-clamp whole-cell recordings used an intracellular solution containing the following (in mM): 135 K-gluconate, 2 MgCl$_2$, 0.1 EGTA, 10 HEPES, 4 KCl, 2 Mg-ATP, 0.5 Na-GTP, 10 phosphocreatine, and 0.2% biocytin, pH 7.3 (314 mOsm). For Figure 7, Na-GTP was excluded from the intracellular solution. Voltage-clamp whole-cell recordings in Figure 3 used an intracellular solution containing the following (in mM): 110 CsCl, 35 CsF, 10 HEPES, 0.1 EGTA, 2 Mg-ATP, 0.5 Na-GTP, and 0.5 QX314, pH 7.2 (310 mOsm). Pipette solutions were adjusted if needed with sucrose to within 5 mOsm of the ACSF.

Adult-born GCs were identified by tdT expression, with cell age approximated from the first day of injections. Mature GCs were defined as unlabeled GCs located in the middle to outer GCL with input resistance between 200 and 400 MΩ, to avoid adult-born GCs and semilunar

GCs (Larimer and Strowbridge, 2010). To monitor formation of stable perforated patches, membrane currents in response to voltage steps were sampled at 20–40 kHz and filtered at 10 kHz. Membrane potentials were sampled at 20–40 kHz and filtered at 2 kHz using Pclamp10 (Digidata 1440A, MultiClamp 700B; Molecular Devices). GCs were recorded from the initial resting membrane potential that did not differ between cell ages (one-way ANOVA). If needed, small current injections were used to maintain constant membrane potential throughout the LTP experiments. Synaptic potentials were evoked using a pipette filled with extracellular solution placed in the middle molecular layer (ML) 200–400 μm from the recorded cell using an isolated current stimulator (Digitimer, 100 μs, 10–100 μA). Series resistance (R_{series}) was monitored throughout experiments and compensated using bridge balance. Experiments were discarded if R_{series} changed by >20%. Voltages were not corrected for junction potentials. Experiments testing pharmacological interventions were interleaved. In Figure 3, IPSCs isolated in NBQX and CPP were evoked by alternate electric and optogenetic stimulation every 30 s. Electrical stimulation was achieved with a pipette placed in the middle (ML; 80–100 μA) or in the granule cell layer (GCL; 40–60 μA). Light stimuli (1 ms) were delivered using a T-Cube LED Driver (LEDD1B, Thor Laboratories) as described in Vaden et al. (2020).

All data were analyzed using AxoGraph X (AxoGraph Scientific) or Clampfit 10.7 (Molecular Devices). Experiments with significant EPSP rundown during the baseline were discarded, but minor sloping baselines were corrected post hoc using AxoGraph sloping baseline correction. Cells with sudden shifts in properties consistent with instability or breakthrough of the perforated patch were excluded from analysis. Rheobase was determined using 10 pA current steps of 500 ms (Fig. 2) or 150 ms current steps of 5 or 10 pA for abGCs and mGCs, respectively (Fig. 4). Rise time was calculated as the 10–90% time to peak, decay time from 80 to 20% of peak, and half-width was calculated at 50% of peak. The paired-pulse ratio (PPR) was measured as the amplitude of EPSP2 subtracted from EPSP1 immediately after the second stimulus. EPSPs were evoked every 20 s (0.05 Hz) and binned into 1 min intervals that were normalized to baseline EPSPs calculated from the average of 10 min prior to theta burst stimulation (TBS). Occasional EPSPs that contained spikes after TBS were excluded from analysis. Action potential bursts (Fig. 4) were defined as initial action potentials with an interspike interval (ISI) < 15 ms using the lowest current injections where the last ISI was ~40 ms.

Drugs. Drugs used included the GABA$_A$ antagonist Gabazine (GBZ; 10 μM), the NMDAR antagonist (R)-CPP (CPP; 5 μM), the AMPAR antagonist NBQX (10 μM), the T-type Ca^{2+} channel blocker TTA-P2 (TTA; 1 μM), and the μ-opioid receptor agonist DAMGO (1 μM). Drugs were purchased from Abcam, Alomone Labs, or Sigma-Aldrich. Other salts and chemicals were purchased from Fischer Scientific.

Statistical analysis. Data are expressed as mean ± SEM. Group comparisons used two-sample paired or unpaired t tests or ANOVA when the number of groups exceeded two, with repeated measures where appropriate. All tests used two-tailed Type I error rate of 0.05 (GraphPad Prism). Data were tested for the assumptions of the respective comparisons. If assumptions were not met, the data were further investigated for outliers. Nonparametric tests were used if data was nonnormal or had significantly different variances due to more than a single outlier. For most multiple comparisons, we used two-way or one-way ANOVAs. The F values were used to express the significant difference or the interaction, and post hoc analyses were made with Sidak's, Bonferroni's, or Tukey's tests. For nonparametric multiple comparisons, a Welsh's test or Kruskal–Wallis' test was used, depending on whether data was non-normal, or if the variance did not meet assumptions, respectively. Post hoc analysis was Dunnett's or Dunn's multiple comparisons. All p and n values are indicated in the text, figures, or figure legends.

Results

To identify abGCs for recording in acute brain slices, we induced tdTomato (tdT) expression in 6-week-old $Ascl1^{CreERT2}$:Ai14 mice with tamoxifen injections (1×/day for 2 d; Yang et al., 2015). At 4, 6, or 8 weeks after tamoxifen, we killed mice for morphological or electrophysiological analysis in horizontal sections containing the intermediate region along the hippocampal septotemporal axis (Fig. 1A). Anatomical reconstructions from fixed brain sections showed that the TDL of abGCs increased between 4 and 8 weeks of cell age with no difference between 6 and 8 weeks (955 ± 51 μm, 1,227 ± 58 μm, 1,332 ± 62 μm, respectively; Fig. 1B). Sholl analysis showed a similar increase in intersections at distal dendritic regions between 4 and 8 weeks (Fig. 1C). These results are consistent with the plateau of dendritic growth that occurs between 4 and 6 weeks after abGC birth (Sun et al., 2013; Goncalves et al., 2016).

Despite the minimal changes in dendrite structure, perforated patch recordings in acute slices revealed more robust changes in GC intrinsic excitability. Four week-old abGCs had an input resistance of 1,012 ± 87 MΩ that declined to 511 ± 57 MΩ at 8 weeks, and all ages were significantly higher than unlabeled mature (M) GCs (270 ± 26 MΩ; Fig. 1D, left). Likewise, abGCs had lower rheobase compared with mature GCs, indicating higher intrinsic excitability (Fig. 1D, right). The membrane time constant of 4w abGCs (44 ± 3 ms) was slower than that of mature GCs (31 ± 2 ms; $p = 0.005$, ANOVA) and the capacitance increased between 4w and 8w (45 ± 2 pF, 66 ± 7 pF, 73 ± 7 pF) and was lower than that in mature GCs (124 ± 12 pF, $p < 0.01$, ANOVA; Dunnett's T3 multiple comparisons). We stimulated the middle ML to evoke EPSPs in GCs located far from the stimulating electrode (Fig. 1E) and adjusted the intensity to elicit EPSPs of similar amplitude (6.5 ± 0.7 mV, 7.3 ± 0.8 mV, 8.1 ± 1.2 mV, 9.8 ± 1.0 mV, respectively; Fig. 1F). Consistent with the high intrinsic excitability of abGCs counteracting low synaptic connectivity (Mongiat et al., 2009; Dieni et al., 2016), the stimulation intensity to elicit EPSPs of similar amplitude did not differ by GC age ($n = 39$; Kruskal–Wallis test; $H_{(3)} = 1.2$, $p = 0.7$). Medial perforant path EPSPs had a similar PPR across cell age (0.79 ± 0.06, 0.85 ± 0.04, 0.98 ± 0.03, 0.97 ± 0.03, respectively; Fig. 1F). As expected from the changes in intrinsic membrane properties, the rise and decay phases of EPSPs differed across cell age with slower rise and decay times in 4w abGCs (Fig. 1G). Thus, the intrinsic properties of abGCs exhibit a gradual maturation that is almost complete by 8 weeks after cell birth (Esposito et al., 2005; Piatti et al., 2011; Dieni et al., 2013).

The critical period for synaptic plasticity

We assessed the critical period for LTP with intact inhibition. After establishing a stable baseline of EPSPs, we applied synaptic TBS paired with postsynaptic current injections to elicit action potentials that mimic GC firing in a place field (Skaggs et al., 1996; Schmidt-Hieber et al., 2004). TBS was repeated 10 times at 5 Hz for a total of 100 stimuli, similar to that observed in vivo (Skaggs et al., 1996). TBS induced LTP so that the averaged EPSP increased to 151 ± 5% and 165 ± 14% of control in 4w and 6w abGCs, respectively. In contrast, TBS had no effect on EPSP amplitudes in 8w abGCs (99 ± 4%) and unlabeled M GCs (96 ± 4%; Fig. 2A,B). Thus, with intact inhibition abGCs transiently exhibit a critical period for LTP that ends between 6 and 8 weeks after cell birth, highlighting the potential capacity for young abGCs to uniquely contribute to plasticity in vivo (Gu et al., 2012).
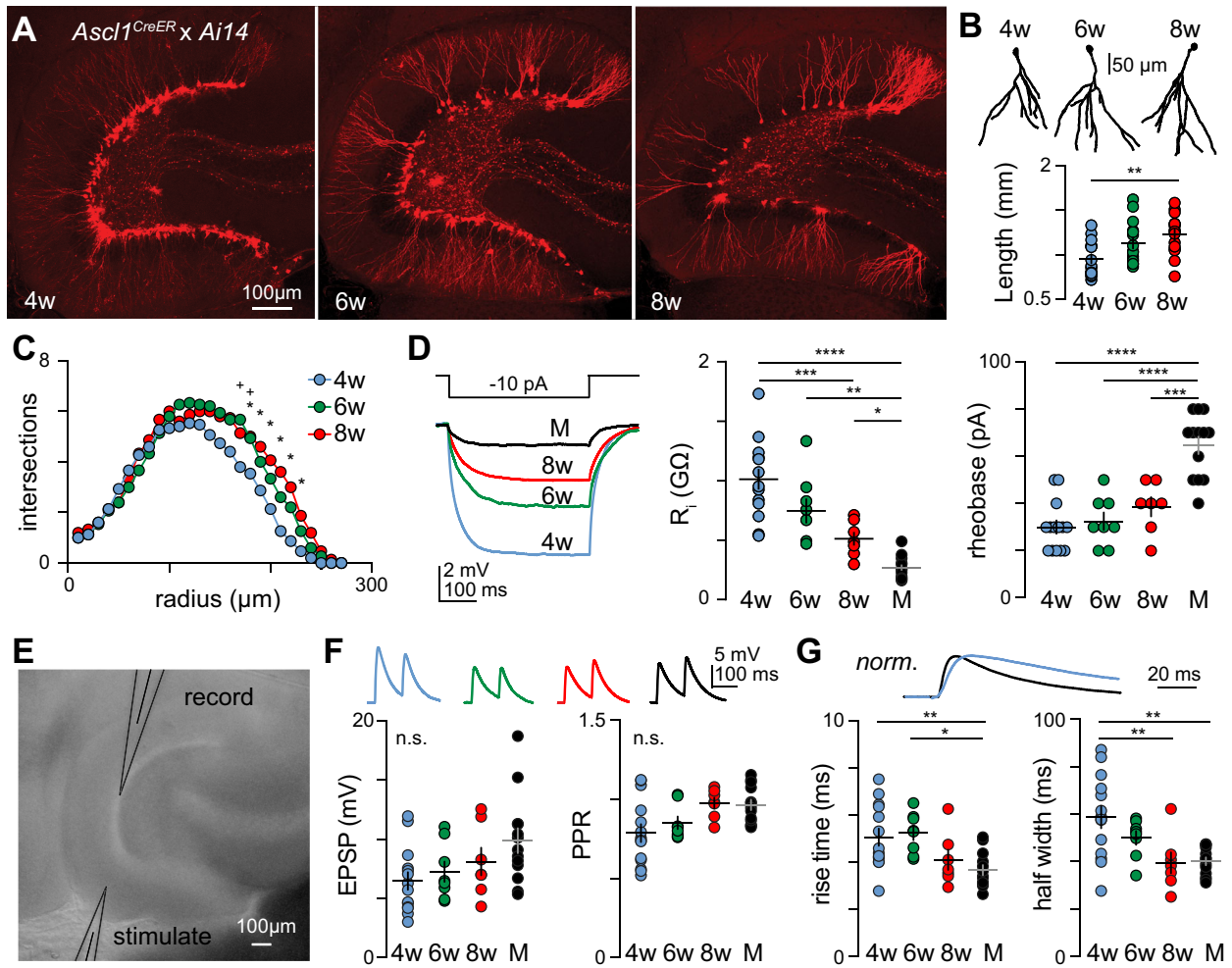
Figure 1. Properties of abGCs. **A**, Confocal images of abGCs from fixed slices (50 μm thick). **B**, Example reconstructions and TDLs ($n = 15$ cells from 2 mice each). One-way ANOVA, $F_{(2,42)} = 5.80$, $p = 0.006$; Tukey's post hoc test 4w versus 8w $p = 0.005$. **C**, Sholl analysis. Two-way ANOVA main effect of cell age, $F_{(2,42)} = 4.2$, $p = 0.02$; main effect of radius, $F_{(26, 1,092)} = 91$, $p < 0.0001$; interaction effect, $F_{(52,1,092)} = 1.54$, $p = 0.009$; Tukey's post hoc test; +, 4w versus 6w $p < 0.05$; *, 4w versus 8w $p < 0.05$. **D**, Left, Examples of hyperpolarization induced by −10 pA current steps. Middle, input resistance (R_i) decreased with cell age. 4w, $n = 14$; 6w, $n = 8$; 8w, $n = 7$; M, $n = 13$; Welch's ANOVA, $F_{(3,0,15.5)} = 27$, $p < 0.0001$; Dunnett's T3 multiple comparisons with 4w versus M $p < 0.0001$, 4w versus 8w $p = 0.0007$, 6w versus M $p = 0.01$, 8w versus M $p = 0.02$. Right, rheobase was lower in abGCs compared to mature GCs, one-way ANOVA, $F_{(3,38)} = 24$, $p < 0.0001$; Dunnett's T3 multiple comparisons. **E**, Live image showing typical recording configuration. **F**, EPSPs had similar amplitude (Kruskal–Wallis test; $H_{(3)} = 7.0$, $p = 0.07$) and PPR (Welch's ANOVA; $W_{(3.0,19)} = 4.1$, $p = 0.02$; Dunnett's multiple comparisons, $p > 0.05$). **G**, Normalized EPSPs highlighting different rise and decay kinetics. Rise: one-way ANOVA; $F_{(3,38)} = 5.5$, $p = 0.003$; Dunnett's T3 multiple comparisons, 4w versus M $p = 0.008$, 6w versus M $p = 0.01$. Half-width: one-way ANOVA $F_{(3,38)} = 6.7$, $p = 0.001$; Tukey's post hoc tests, 4w versus M $p = 0.002$, 4w versus 8w $p = 0.008$. n.s., not significant, *$p < 0.05$, **$p < 0.01$, ***$p < 0.001$, ****$p < 0.0001$. All error bars ± SEM.

In contrast to the NMDAR-dependent postsynaptic mechanism of LTP at medial perforant path synapses (Ge et al., 2007), lateral perforant path synapses exhibit presynaptic plasticity resulting from an increase in vesicular release probability (Wang et al., 2016; Vyleta and Snyder, 2021). To confirm plasticity was generated at medial perforant path synapses, we used paired stimuli (0.05 Hz, 100 ms ISI) throughout most experiments to assess the PPR that is associated with changes in the probability of release (Fig. 2C) and found no differences at 25 min post-TBS (two-way ANOVA; TBS $F_{(1,22)} = 2.0$ $p = 0.2$). To test whether plasticity of intrinsic properties rather than synaptic conductances could potentiate EPSPs (Lopez-Rojas et al., 2016; Mishra and Narayanan, 2022), we monitored rheobase before and after LTP induction. There was no effect of TBS on rheobase, however, mature GCs exhibited higher rheobase consistent with lower excitability (Fig. 2D). Together these results confirm that 4w and 6w abGCs exhibit a high propensity for postsynaptic LTP at medial perforant path synapses similar to

the reported timing of the critical period with GABA_A receptor-mediated inhibition blocked (Ge et al., 2007).

GABAergic inhibition suppresses LTP in both mature and young GCs

We tested whether minimal GABAergic inhibition contributes to the high propensity for LTP in abGCs by blocking GABA_A receptors with GBZ (10 μM). We reasoned that if minimal inhibition underlies critical period plasticity, then LTP in 4w abGCs will be relatively insensitive to removing inhibition. As a positive control, we first confirmed that our perforant path stimuli effectively recruits inhibition by showing that GBZ increases the amplitude of baseline EPSPs in both mature ($137 ± 13\%$; paired t tests; $t_{(3)} = 4.1$, $p = 0.03$; $n = 4$) and 4w abGCs ($128 ± 8\%$; paired t test; $t_{(2)} = 4.85$, $p = 0.04$; $n = 3$; data not shown). We then repeated LTP experiments in the presence of GBZ. As expected, GBZ uncovered LTP in mature GCs, resulting in EPSPs that were ~160% of the pre-TBS baseline (Fig. 3A, left). In contrast to the idea
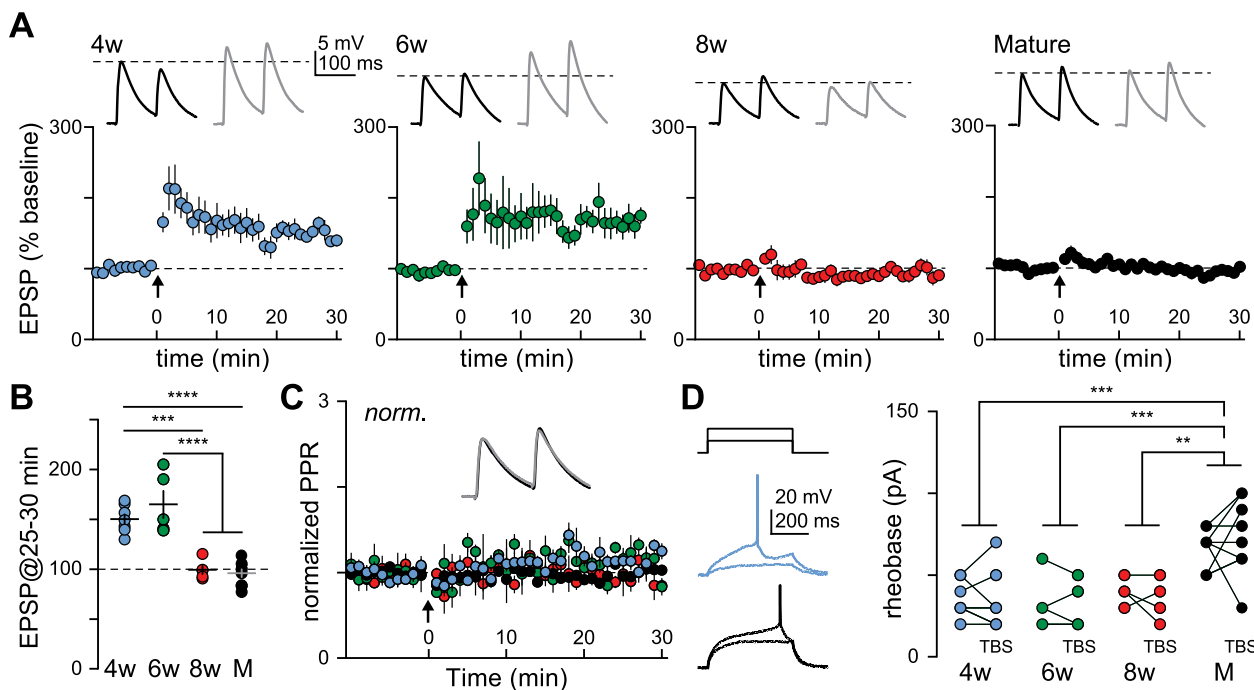
Figure 2. The critical period for synaptic plasticity. ***A***, EPSPs in perforated patch recordings from GCs at each age were normalized during a 10 min baseline before TBS and binned into 1 min intervals. Insets show example EPSPs before and after TBS. Dotted lines mark baseline. ***B***, Comparison of EPSPs at 25–30 min post-TBS. 4w, $n = 7$; 6w, $n = 5$; 8w, $n = 5$; M, $n = 9$; one-way ANOVA; $F_{(3,23)} = 26$, $p < 0.0001$; Tukey's post hoc with 4w versus M $p < 0.0001$, 4w versus 8w $p = 0.0002$, 6w versus 8w and M $p < 0.0001$. ***C***, PPRs normalized and binned. Inset shows example EPSPs from a 6w abGC. ***D***, Current injections used to monitor rheobase before and after TBS from a 4w (blue, 20 and 30 pA) and mature GC (black, 50 and 60 pA). TBS did not alter rheobase (2-way ANOVA; $F_{(1,22)} = 0.01$, $p = 0.9$), but rheobase was higher in mature GCs compared with abGCs ($F_{(3,22)} = 14$, $p < 0.0001$; Tukey's post hoc with 4w versus M $p = 0.0001$, 6w versus M $p = 0.0002$, 8w versus M 0.004, and no interaction effect ($F_{(3,22)} = 0.61$, $p = 0.6$). 4w, $n = 7$; 6w, $n = 5$; 8w, $n = 4$; M, $n = 9$.

that plasticity in abGCs is insensitive to inhibition, the EPSP amplitudes in 4w abGCs were ∼280% of the pre-TBS baseline in GBZ (Fig. 3*A*, right). Note that baseline EPSPs evoked in GBZ using the same stimulation intensity (unpaired *t* test; $t_{(9)} = 0.78$, $p = 0.5$) generated smaller EPSPs in 4w abGCs compared with those in mature GCs (6.1 ± 0.4 mV vs 9.8 ± 0.8 mV; unpaired *t* test; $t_{(9)} = 3.57$, $p = 0.005$; data not shown), consistent with sparse excitatory synaptic connectivity (Dieni et al., 2016). GBZ increased the effect of TBS in both mature and 4w abGCs, with a significant interaction between cell age and GBZ suggesting a larger effect of GBZ in 4w abGCs compared with that in mature GCs (Fig. 3*B*, left). We also compared the relative effect of GBZ on plasticity in 4w and mature GCs by the ratio of LTP in GBZ versus LTP in ACSF, using the %EPSP after TBS from individual experiments in GBZ and the average %EPSP after TBS in ACSF. This ratio suggests GBZ had a similar effect in mature and 4w GCs (1.67 ± 0.22 and 1.85 ± 0.04; unpaired Welch's *t* test; $t_{(5.3)} = 0.78$, $p = 0.5$; Fig. 3*B*, right). Variability in the effect of GBZ in mature GCs could result from variability in I/E ratios (Dieni et al., 2013) and/or vulnerability of interneurons in the slice. Nonetheless, these results contradict the hypothesis that minimal inhibition underlies critical period plasticity, by showing that inhibition strongly suppresses LTP in 4w abGCs and suggesting that the relative effect of GBZ in 4w abGCs is similar to, or greater rather than less than, the effect in mature GCs.

To further investigate the unexpectedly strong effect of GBZ in 4w abGCs, we compared its effect on depolarization induced by single bursts of 100 Hz synaptic stimulation used in the TBS (in the absence of postsynaptic current injections that impede identification of synaptic potentials). We used whole-cell recordings to equalize intracellular [Cl⁻] and reduce series resistance, focusing on 6w abGCs that are well past the maturation of the chloride equilibrium potential (Ge et al., 2006) yet still exhibit robust LTP (Fig. 2). Once again, we adjusted the stimulation intensity to elicit EPSPs with similar amplitude (6w, 9.7 ± 1.1 mV; M, 9.6 ± 0.9 mV; unpaired *t* test; $t_{(12)} = 0.056$, $p = 0.96$) using a similar stimulation intensity (36 ± 6 µA vs 28 ± 5 µA; unpaired *t* test; $t_{(11)} = 0.97$, $p = 0.4$). Synaptic TBS generated similar depolarization in 6w and mature GCs, and both were increased to a similar degree by GBZ, measured either as the total area or maximal amplitude (Fig. 3*C*). Thus, despite incomplete innervation from PV and SST interneurons (Groisman et al., 2020), inhibition during the critical period effectively suppresses depolarization during repetitive synaptic stimulation. Whereas blocking GABA_A receptors enhances depolarization in mature GCs sufficiently to reach threshold for LTP, it enhances the magnitude of LTP in young GCs.

To avoid potential confounds resulting from complete blockade of GABA_A receptors, we tested the sensitivity of critical period plasticity to partial block of GABA release. In CA1, µ-opioid receptors (µORs) are expressed selectively on GABAergic interneurons, where they suppress GABA release from neurogliaform and PV interneurons, but not CCK interneurons (Glickfeld et al., 2008; Krook-Magnuson et al., 2011). To confirm partial suppression of GABA release in dentate gyrus, we tested the effect of the µOR agonist DAMGO (1 µM) on optogenetic-evoked GABA_A receptor-mediated IPSCs in mature GCs. DAMGO strongly reduced IPSCs evoked by optogenetic activation of nNos-expressing interneurons, a group of dendritic-projecting interneurons that include neurogliaform cells (Gonzalez et al., 2018; Vaden et al., 2020). IPSCs evoked by nNos interneurons
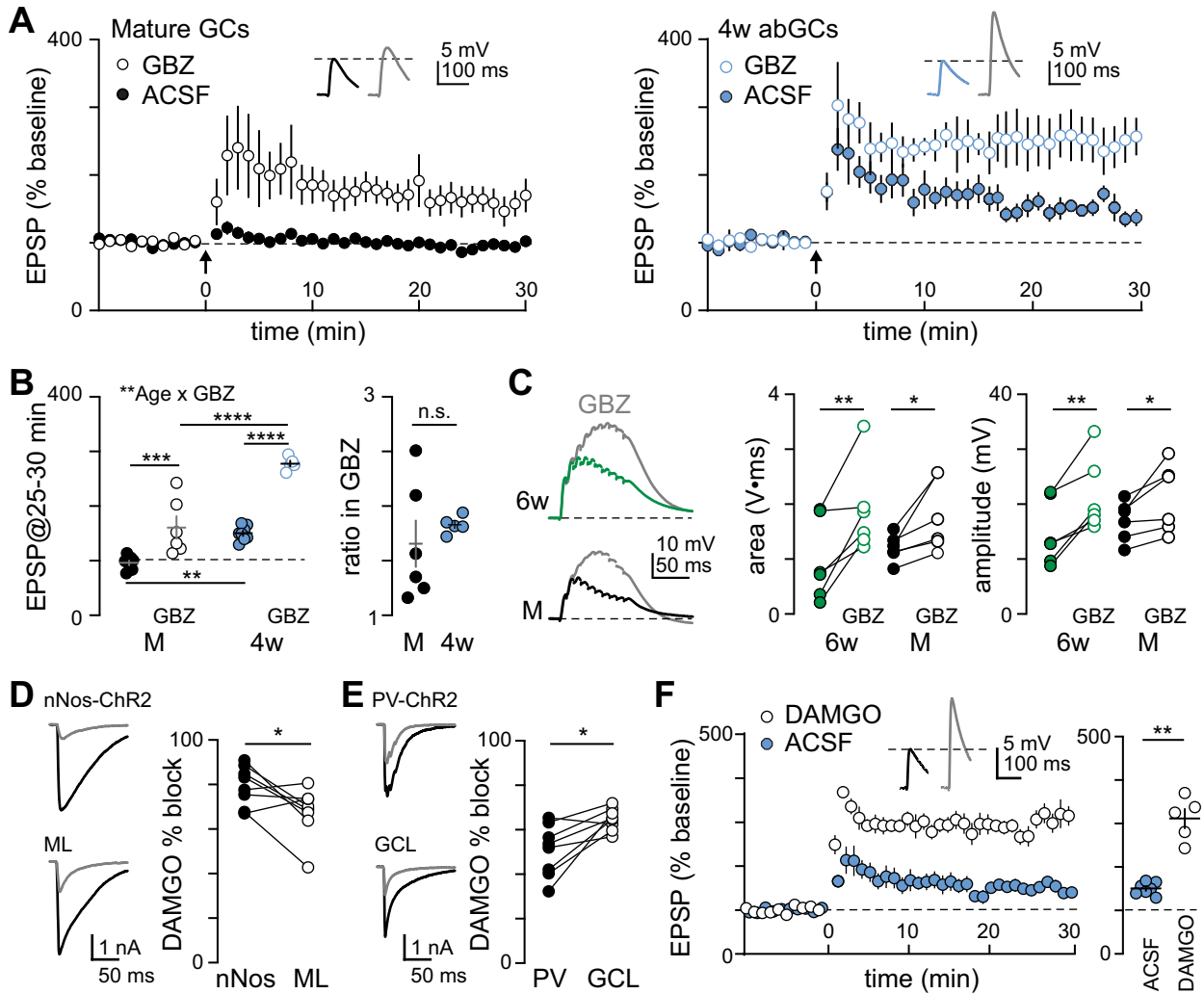
Figure 3. GABA$_A$R-mediated inhibition suppresses LTP. **A**, LTP in perforated patch recordings from mature GCs ($n = 6$; left) and 4w abGCs ($n = 5$; right) in GBZ (open symbols), with comparison to results in ACSF (from Fig. 2A, solid symbols). Insets show EPSPs before and after TBS in GBZ. **B**, Left, Summary data from 25 to 30 min post-TBS. Two-way ANOVA main effect of cell age $p < 0.0001$; main effect of GBZ $p < 0.0001$; interaction effect $F_{(1,24)} = 10$, $p = 0.005$; Tukey's post hoc 4w ACSF versus GBZ $p < 0.0001$, 4w ACSF versus M ACSF $p = 0.001$, 4w GBZ versus M GBZ $p < 0.0001$, M ACSF versus GBZ $p = 0.0004$. Right, The ratio of LTP in GBZ versus ACSF; unpaired Welch's t test; $t_{(5.3)} = 0.78$, $p = 0.5$) **C**, Example depolarizations in 6w or M GCs during TBS using whole-cell recordings ($n = 6$ each). GBZ increases the area ($p = 0.0007$) regardless of cell age ($p = 0.7$). There was no significant interaction effect between cell age and GBZ (two-way RM ANOVA; $F_{(1,10)} = 1.2$, $p = 0.3$; Bonferroni's multiple comparisons 6w $p = 0.004$, M $p = 0.048$). GBZ also increases the peak amplitude of depolarization. Two-way RM ANOVA, $F_{(1,10)} = 1.7$, $p = 0.2$; main effect of cell age $p = 0.8$; main effect of GBZ $p = 0.0003$; Bonferroni's multiple comparisons 6w $p = 0.002$, M $p = 0.04$. **D**, IPSCs in mature GCs evoked by alternating optogenetic stimulation of nNos-ChR2 (top, 1 ms) and electrical stimulation in the ML (bottom) were reduced by DAMGO (gray). Paired t test; $t_{(7)} = 2.61$, $p = 0.03$ ($n = 8$). **E**, IPSCs evoked by alternating optogenetic stimulation of PV-ChR2 and electrical stimulation in the GCL (bottom), were suppressed by DAMGO. Paired t test; $t_{(7)} = 3.39$, $p = 0.01$ ($n = 8$). **F**, DAMGO enhanced LTP in perforated patch recordings from 4w abGCs ($312 \pm 22\%$; $n = 5$; perforated patch recordings) compared with ACSF (from Fig. 2A; Welch's t test; $t_{(4.5)} = 7.0$ $p = 0.001$).

were reduced to a greater extent than IPSCs evoked by nonselective electrical stimulation of the ML (by $79.4 \pm 3.2\%$ vs $67.6 \pm 4.0\%$; Fig. 3D). DAMGO also reduced IPSCs evoked by optogenetic stimulation of PV interneurons, but to a lesser extent than IPSCs evoked by nonselective electrical stimulation near the GCL ($50.7 \pm 4.1\%$ vs $64.7 \pm 1.8\%$; Fig. 3E). Thus, DAMGO reduces GABA release from nNos and PV interneurons but presumably leaves release intact from other subtypes, allowing us to test how partial suppression of inhibition affects LTP. Consistent with μOR expression primarily in nNos and PV interneurons, DAMGO had no detectable effect on the intrinsic properties of 4w abGCs in perforated patch recordings (data not shown; $n = 5$). However, DAMGO robustly facilitated LTP, resulting in a magnitude of LTP that was greater than in ACSF ($312 \pm 22\%$ vs $151 \pm 5\%$; Fig. 3F). Thus, a partial reduction of GABAergic inhibition resulting from suppression of GABA release enhances LTP

in abGCs. Altogether these experiments reveal multiple outcomes inconsistent with the idea that minimal GABAergic transmission underlies critical period plasticity.

T-type Ca^{2+} channel antagonist sensitivity correlates with critical period LTP

In addition to changes in synaptic connectivity, the closure of the critical period is accompanied by reduced intrinsic excitability resulting from changes in the complement, density, and/or function of multiple ion channels (Esposito et al., 2005; Overstreet-Wadiche et al., 2006; Mongiat et al., 2009). In particular, young abGCs with enhanced synaptic plasticity also exhibit T-type Ca^{2+} spikelets that facilitate depolarization to threshold for Na$^+$-dependent action potentials (Schmidt-Hieber et al., 2004). We found that the incidence of putative Ca^{2+} spikelets in response to subthreshold current injections in the LTP
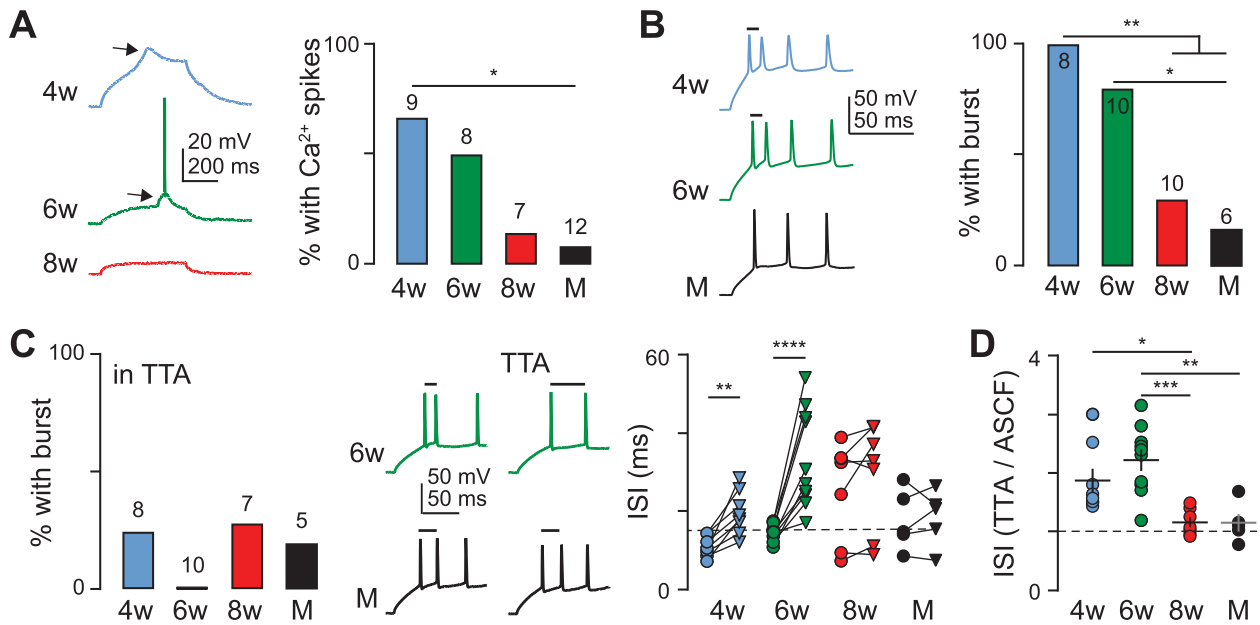
Figure 4. Sensitivity to T-type Ca^{2+} channel antagonist correlates with the critical period. ***A***, Examples of putative T-type Ca^{2+} spikelets (arrows) in 4w and 6w abGCs from perforated patch recordings. The spikelet reaches threshold for a Na$^+$ action potential in the 6w abGC. Multiple Fisher's exact tests, 4w versus M $p = 0.02$. Total number of cells as indicated. ***B***, Typical firing patterns in whole-cell recordings, with action potential bursts indicated by lines. Multiple Fisher's exact tests. 4w versus 8w and M $p = 0.003$, 6w versus M $p = 0.04$. ***C***, Left, Percent of cells in TTA with bursts. Multiple Fisher's exact tests, not significant. Middle, Example firing patterns with first spike ISIs indicated in control (left) and TTA (right). Right, ISI in ACSF (circles) and TTA (triangles). Dotted line indicates ISI of 15 ms. Two-way RM ANOVA main effect cell age, $F_{(3,26)} = 3.0$, $p = 0.048$; main effect TTA, $F_{(1,26)} = 27$, $p < 0.0001$; interaction effect, $F_{(3,26)} = 9.06$, $p = 0.0003$; Bonferroni's multiple comparisons, 4w $p = 0.004$, 6w $p < 0.0001$. ***D***, The ISI in TTA relative to the ISI in ACSF (dotted line). One-way ANOVA $F_{(3,26)} = 9.2$ $p = 0.0002$; Tukey's post hoc comparison, 4w versus 8w $p = 0.04$, 6w versus 8w $p = 0.0008$, 6w versus M $p = 0.002$. 4w, $n = 8$; 6w, $n = 10$; 8w, $n = 7$; M, $n = 5$.

experiments declined with cell age (67% of 4w abGCs, 50% of 6w abGCs, 14% of 8w abGCs, and 8% of mature GCs; Fig. 4*A*). We thus sought to test the role of T-type channels in critical period plasticity.

To confirm the involvement of T-type Ca^{2+} channels, we intended to test the sensitivity of spikelets to a T-type channel antagonist, but we did not detect many using whole-cell recordings, suggesting reliance on intracellular components that can be diluted. We therefore used a different assay of T-type Ca^{2+} channel activity previously described in whole-cell recordings. T-type Ca^{2+} channels contribute to high-frequency bursts of 2–4 Na$^+$ action potentials at the beginning of suprathreshold current injections, and these bursts correlate with LTP (Dumenieu et al., 2018; Kim et al., 2023). We defined these bursts as spike doublets with a first ISI <15 ms (see Materials and Methods) and found that the incidence of bursts in whole-cell recordings declined with cell maturation (Fig. 4*B*). We confirmed that bursts depend on T-type Ca^{2+} channels using the selective T-type channel blocker TTA-P2 (TTA; 1 µM) (Dreyfus et al., 2010). In TTA, there was no difference in the low incidence of bursts across cell age (Fig. 4*C*, left). TTA increased the first ISI in 4w (from 11 ± 1 to 19 ± 2 ms) and 6w abGCs (from 14 ± 0.5 to 31 ± 3 ms) but had no effect in 8w abGCs (from 24 ± 5 to 27 ± 5 ms) and mature GCs (from 20 ± 3 to 22 ± 2 ms; Fig. 4*C*, middle, right). To compare the sensitivity to TTA across GC age without using a predefined burst criterion, we normalized the ISI in TTA to the ISI in ACSF. We found that 4w abGCs showed a greater increase in ISI (1.9 ± 0.2) compared with 8w abGCs (1.2 ± 0.1) and that 6w abGCs showed a greater increase in ISI (2.2 ± 0.2) compared with 8w and mature GCs (1.1 ± 0.1 and 1.1 ± 0.2; Fig. 4*D*). Thus, 4–6w abGCs in the critical period exhibit a contribution of T-type Ca^{2+} channels to excitability, and the loss of sensitivity to the T-type blocker coincides with the closure of the critical period.

T-type Ca^{2+} channels in abGCs enhance NMDAR-mediated depolarization

We wondered whether T-type Ca^{2+} channel activity could contribute to NMDAR activation reported to be important for critical period plasticity (Ge et al., 2007; Kheirbek et al., 2012). To test this idea, we used whole-cell recordings and the NMDAR antagonist CPP (5 µM) to isolate the NMDAR-mediated component of depolarization during bursts of 100 Hz synaptic stimulation used in the TBS. With EPSPs of similar initial amplitude, the envelope of depolarization generated by 100 Hz stimulation in ACSF in 4w (1.40 ± 0.06 V•ms) and 6w abGCs (1.35 ± 0.09 V•ms; data not shown) was similar to mature GCs (1.32 ± 0.04 V•ms), and CPP reduced it to the same extent (Fig. 5*Ai,iii*). Thus, the area of the isolated NMDAR depolarization was also similar in 4w abGCs (0.56 ± 0.07 V•ms), 6w abGCs (0.35 ± 0.05 V•ms; data not shown), and mature GCs (0.43 ± 0.03 V•ms; one-way ANOVA; $F_{(2,18)} = 1.7$, $p = 0.2$; Fig. 5*Bi,iii*). These results suggest TBS generates similar NMDAR activation in abGCs and mature GCs, although somatic recordings could mask sublinear integration in developing thin dendrites (Abrahamsson et al., 2012). To test the contribution of T-type Ca^{2+} channels to NMDAR activation, we repeated this analysis after blocking T-type Ca^{2+} channels with TTA. In separate experiments, TTA first reduced the area of depolarization in 4w abGCs (from 1.42 ± 0.08 V•ms to 1.12 ± 0.10 V•ms; paired t test; $t_{(8)} = 5.99$, $p = 0.0003$; $n = 9$; data not shown) but had no effect in mature GCs (from 1.35 ± 0.18 V•ms to 1.24 ± 0.15 V•ms; paired t test; $t_{(6)} = 1.47$, $p = 0.2$; $n = 6$, not shown), consistent with selective effects on excitability in abGCs. We then tested CPP in the presence of TTA. In 4w abGCs, there was no additional effect of CPP (from 1.12 ± 0.10 V•ms to 1.11 ± 0.12 V•ms; Fig. 5*Aii*), in contrast to the block by CPP in ACSF alone (from 1.40 ± 0.06 V•ms to 0.84 ± 0.08 V•ms; Fig. 5*Ai*). In mature GCs, CPP
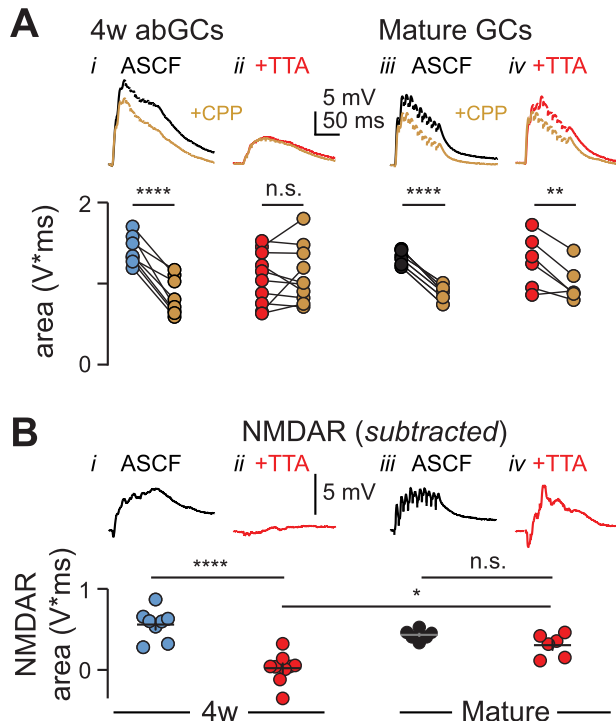
Figure 5. T-type Ca^{2+} channels enhance NMDAR-mediated depolarization. *A*, Depolarization in whole-cell recordings during 100 Hz synaptic stimulation in ACSF (black) and CPP (brown) in 4w (*i*) and mature GCs (*iii*). CPP blocked depolarization to a similar extent in 4w, 6w (data not shown), and mature GCs (2-way RM ANOVA, $F_{(2,18)} = 4.5$, $p = 0.03$; main effect of CPP, $p < 0.0001$; cell age, $p = 0.97$; Bonferroni's multiple comparisons, 4w, 6w, and M $p < 0.0001$). Comparison of the effect of CPP in ASCF (*i,iii*) with effect of CPP in the presence of TTA (*ii,iv*) revealed that CPP blocked depolarization, dependent on TTA (2-way ANOVA cell condition × CPP, $F_{(3,26)} = 16.4$, $p < 0.0001$; main effect of cell condition, $p = 1$; main effect of CPP, $p < 0.0001$; Bonferroni's multiple comparisons, 4w and M ASCF $p < 0.0001$, M TTA $p = 0.002$). *B*, The subtracted NMDAR-mediated components were similar in 4w (*i*), 6w (data not shown), and mature GCs (*iii*; 1-way ANOVA, $F_{(2,18)} = 1.7$, $p = 0.2$). In 4w abGCs, the subtracted NMDA component was smaller in TTA (*ii*) than in ACSF (*i*), whereas in mature GCs the NMDAR component was similar in ACSF (*iii*) and TTA (*iv*; 1-way ANOVA, $F_{(3,25)} = 18$, $p < 0.0001$; Bonferroni's multiple comparisons, 4w ACSF versus TTA $p < 0.0001$, 4w TTA versus M TTA $p = 0.01$, M ACSF versus TTA $p = 0.7$). 6w ACSF, $n = 7$; 4w ACSF, $n = 8$; 4w TTA, $n = 9$; M ACSF, $n = 6$; M TTA, $n = 6$.

reduced the depolarization in the presence of TTA (from 1.24 ± 0.15 V•ms to 0.94 ± 0.12 V•ms; Fig. 5A*iv*), similar to the effect of CPP in ACSF (from 1.32 ± 0.04 V•ms to 0.89 ± 0.04 V•ms; Fig. 5A*iii*). We used these experiments to directly compare the effect of TTA on the subtracted NMDAR component. In 4w abGCs, the NMDAR component in TTA was smaller than that in ACSF (0.02 ± 0.06 V•ms vs 0.56 ± 0.07 V•ms; Fig. 5B*i,ii*), but TTA had no effect on the NMDAR component in mature GCs (from 0.43 ± 0.03 V•ms to 0.31 ± 0.06 V•ms; Fig. 5B*iii,iv*). In TTA, the NMDAR component in 4w abGCs was also smaller than the NMDAR component in mature GCs (Fig. 5B*ii,iv*). Together these results show that T-type Ca^{2+} channels promote NMDAR-mediated depolarization in 4w GCs, and this facilitation does not occur in mature GCs.

T-type Ca^{2+} channels are allow abGCs to overcome inhibition
To directly determine whether T-type Ca^{2+} channels underlie critical period plasticity, we tested the effect of TTA on LTP in 4w abGCs. In contrast to LTP in ACSF (150 ± 5% of control, from Fig. 2), LTP was absent in TTA (86 ± 9% of control; Fig. 6A, left, B), suggesting that T-type Ca^{2+} channels are

necessary for LTP. One caveat, however, is that TTA could suppress LTP by altering GABAergic inhibition. Therefore, we also tested TTA in the presence of GBZ and found that TTA reduced LTP when GABA$_A$ receptors are blocked (GBZ + TTA 153 ± 17% compared with GBZ 278 ± 5%, from Fig. 3; Fig. 6A, middle, B). If TTA suppressed LTP via circuit effects independent of abGCs, then TTA should also prevent LTP in mature GCs in the presence of GBZ. However, TTA did not alter LTP in mature GCs when inhibition was blocked (GBZ 161 ± 21%, Fig. 3; GBZ + TTA 155 ± 22%; $p = 0.8$; Fig. 6A, right, B). In these experiments, we used similar initial EPSP amplitudes and stimulation intensities (see legend). Comparing across all conditions, we found that TTA affected LTP only in 4w abGCs and that when both GABA$_A$ receptors and T-type Ca^{2+} channels are blocked, the magnitude of LTP was similar in 4w abGCs and mature GCs (Fig. 6B). This implies that the primary difference is the enhanced excitability afforded by T-type Ca^{2+} channels that allow abGCs to overcome the suppressive effect of inhibition but that T-type Ca^{2+} are not strictly required for LTP in either young or mature GCs.

In these perforated patch recordings, we noticed that the time course of single EPSPs in 4w abGCs was accelerated by TTA, both in ACSF and in GBZ (EPSP half-width in ACSF 59 ± 5 ms compared with 33 ± 4 ms in TTA, in GBZ 70 ± 5 ms compared with 50 ± 6 in GBZ + TTA; Fig. 6C). Thus, even single synaptic stimuli activate T-type Ca^{2+} channels that promote depolarization in 4w abGCs, but TTA had no effect on the time course of EPSPs in mature GCs (EPSP half-width in GBZ 40 ± 2 ms compared with 38 ± 4 ms in GBZ + TTA; Fig. 6C). Likewise, we also confirmed that TTA selectively increased the intrinsic excitability of young abGCs, showing that TTA decreased the number of action potentials generated by either short (150 ms, Fig. 6D) or long (500 ms, Fig. 6E) current injections. Altogether these results suggest that T-type Ca^{2+} channels mediate critical period LTP in young abGCs via cell autonomous effect on intrinsic excitability.

Uncovering T-type Ca^{2+} channels in mature GCs unmasks LTP
Our results suggest that the closure of critical period plasticity corresponds to the loss of T-type Ca^{2+} channel-mediated excitability. However, whole-cell recordings show that T-type-dependent burst firing correlates with various forms of LTP in GCs with mature properties in juvenile rat slices (Kim et al., 2023) and past work clearly identifies T-type Ca^{2+} channel activity in mature GCs (Beck et al., 1998; Martinello et al., 2015; Dumenieu et al., 2018). Thus, loss of T-type Ca^{2+} channel excitability does not result from loss of channel expression. We previously showed that constitutive G-protein signaling suppresses intrinsic excitability of mature but not newborn GCs and that excluding GTP from the intracellular solution increases mature GC intrinsic excitability and bursting (Gonzalez et al., 2018, 2023). Therefore, we tested whether suppressing G-protein signaling could unmask T-type Ca^{2+} channel activity in mature GCs and uncover LTP with intact synaptic inhibition.

First, we used whole-cell recordings from mature GCs with no intracellular GTP to assay T-type Ca^{2+} channel contribution to spike bursts. After 5 min to allow the intracellular solution lacking GTP to diffuse into the cell, we tested the effect of TTA on the ISI of the first spikes generated by current injections. In contrast to whole-cell recordings with GTP (Fig. 4B), most mature GCs showed a spike burst (75%) in the absence of intracellular GTP, as reported (Gonzalez et al., 2023). Furthermore, TTA increased the ISI of the doublet, confirming a contribution of T-type Ca^{2+} channels to this form of intrinsic excitability (from
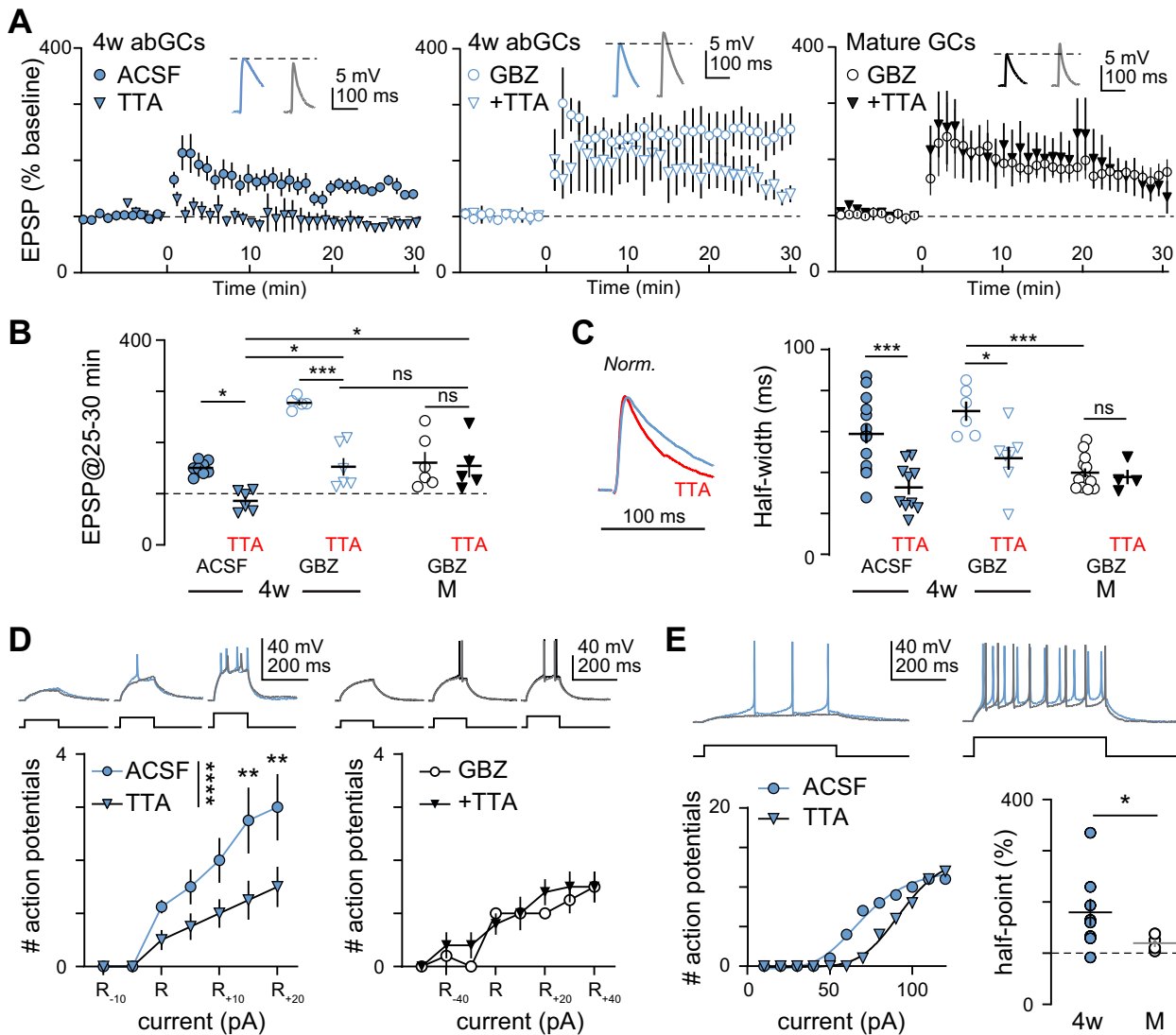
Figure 6. T-type Ca^{2+} channels allow abGCs to overcome inhibition. **A**, Left, LTP induction in 4w abGCs in ACSF (circles; data from Fig. 2) and TTA (triangles; $n = 6$) in perforated patch recordings. Middle, LTP induction in 4w abGCs in GBZ (circles; data from Fig. 3) and GBZ + TTA (triangles; $n = 6$). Right, LTP in M GCs in GBZ (circles; data from Fig. 3) and GBZ + TTA (triangles; $n = 5$). All insets, example EPSPs before and after TBS in TTA. Initial EPSP amplitudes (4w ACSF, 7 ± 1 mV; 4w TTA, 9 ± 2 mV; 4w GBZ, 6 ± 0.4 mV; 4w GBZ + TTA, 6 ± 1 mV; M GBZ, 10 ± 1 mV; M GBZ + TTA, 6 ± 0.5 mV; one-way ANOVA, $F_{(5,29)} = 2.1$, $p = 0.09$) and stimulation intensities (4w ACSF, 22 ± 5 µA; 4w TTA, 22 ± 6 µA; 4w GBZ, 23 ± 6 µA; 4w GBZ + TTA, 26 ± 3 µA; M GBZ, 18 ± 2 µA; M GBZ + TTA, 34 ± 6 µA; Kruskal–Wallis test; $H_{(5)} = 7.4$, $p = 0.2$) were similar across all experiments. **B**, Summary of EPSPs at 25–30 min post-TBS. One-way ANOVA, $F_{(5,30)} = 17$, $p < 0.0001$; Sidak's multiple comparison, 4w ACSF versus 4w TTA $*p = 0.01$, 4w GBZ versus 4w GBZ + TTA $***p < 0.0001$, M GBZ versus M GBZ + TTA $p = 0.99$, 4w TTA versus 4w GBZ + TTA $*p = 0.01$, M TTA versus 4w TTA $*p = 0.02$, 4w GBZ + TTA versus M TTA $p > 0.99$. **C**, Example EPSPs from a 4w abGC in ACSF (blue) and TTA (red). Right, Summary of EPSP half-widths. One-way ANOVA, $F_{(5,49)} = 9.4$, $p < 0.0001$; Sidak's multiple comparisons, 4w ACSF versus 4w TTA $***p < 0.0001$, 4w GBZ versus 4w GBZ + TTA $*p = 0.04$, M GBZ versus M GBZ + TTA $p > 0.99$, 4w TTA versus 4w GBZ + TTA $p = 0.04$. 4w GBZ versus M GBZ $***p = 0.0002$. **D**, Left, Action potentials in response to current injections (5 pA increments) in 4w abGCs in ACSF and TTA (gray), normalized to rheobase (R): two-way RM ANOVA main effect of TTA, $F_{(1,49)} = 24$, $****p < 0.0001$; main effect of current injection, $F_{(6,49)} = 12$, $p < 0.0001$; interaction effect, $F_{(6,49)} = 2.3$, $p = 0.05$; Bonferroni's multiple comparisons, $**p = 0.005$). Right, Similar analysis for mature GCs in GBZ using 10 pA current injections. Two-way RM ANOVA main effect of TTA, $F_{(1,30)} = 1.8$, $p = 0.2$; main effect of current injection, $F_{(7,30)} = 16$, $p < 0.0001$; interaction effect, $F_{(7,30)} = 0.64$, $p = 0.7$. **E**, Top, Action potentials in response to current injections in abGCs in ACSF and TTA (gray). Bottom, the number of action potentials in an abGC normalized to the maximum and fit with a least squares sigmoidal line, illustrating a shift in the half-point by TTA. Summary of the half-point in TTA as a percent of half-point in ACSF. Welch's t test, $t_{(8.1)} = 2.4$, $*p = 0.04$.

10.6 ± 1.4 ms to 13.9 ± 2.0 ms; Fig. 7A). In separate whole-cell recordings from mature GCs, we evoked EPSPs in ACSF or TTA and applied TBS within 15 min of breaking into the cell, using similar initial EPSP amplitudes (ACSF, 10 ± 1 mV; TTA, 8 ± 1 mV) and stimulation intensities (ACSF, 19 ± 2 µA; TTA, 20 ± 2 µA). Remarkably, using whole-cell recordings without GTP generated a robust LTP in ACSF ($222 \pm 17\%$) that was reduced by TTA ($158 \pm 15\%$; Fig. 7B). In these recordings, we also confirmed that the ISI of the doublet in response to current

injection was enhanced by TTA (ISI in ACSF 11 ± 1 ms, ISI in TTA 19 ± 2 ms; unpaired t test; $t_{(12)} = 3.6$, $p = 0.004$). However, even in whole-cell recordings without GTP, TTA did not affect the duration of EPSPs measured by the half-width (39.0 ± 1.7 ms vs 39.9 ± 2.5 ms; unpaired t test; $t_{(11)} = 0.3$, $p = 0.7$). These data suggest that enhancing the contribution of T-type Ca^{2+} channels to intrinsic excitability in mature GCs by suppressing G-protein signaling can unmask a T-type Ca^{2+} channel-dependent component of LTP.
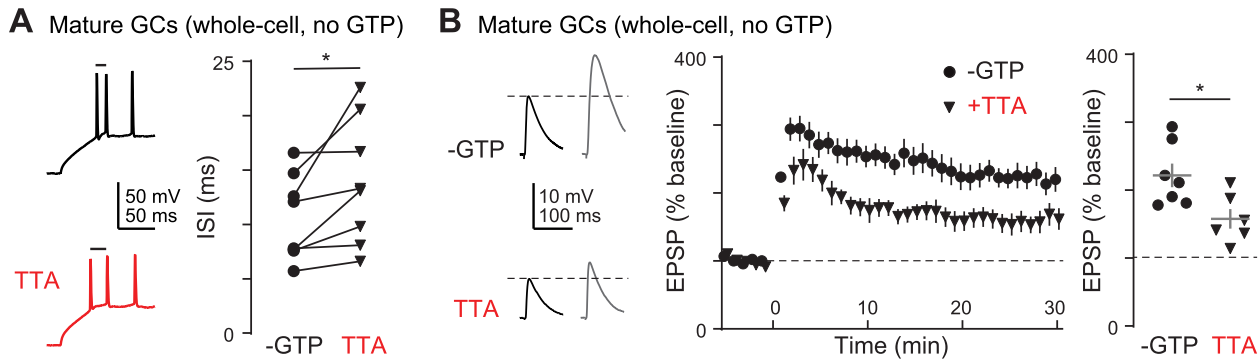
A Mature GCs (whole-cell, no GTP)   **B** Mature GCs (whole-cell, no GTP)

Figure 7. Whole-cell recordings without GTP uncover T-type Ca^{2+} channel contribution to mature GC excitability and LTP. *A*, Example first ISIs in response to current injections 5 min after breaking into a mature GC without GTP in the pipette, before (above) and after TTA application (below). Right, Paired *t* test, $t_{(7)} = 2.6$ **p* = 0.03. *n* = 8. *B*, Example EPSPs in mature GCs in ACSF (top) or TTA (bottom) without GTP in the pipette before and after TBS. Middle, When GTP is excluded from the recording pipette, mature GCs exhibit robust LTP with inhibition intact (*n* = 7) that is sensitive to TTA (*n* = 6). Right, Summary of EPSP amplitudes at 25–30 min post-TBS, unpaired *t* test, $t_{(11)} = 2.8$, **p* = 0.02.

Discussion

In the first 4 weeks after cell birth, abGCs undergo extensive morphological growth and synaptic integration followed by 2 weeks of enhanced synaptic plasticity termed the critical period (Ge et al., 2007). During this critical period, young abGCs have few but highly plastic synapses that provide a substrate for memory precision, likely by promoting functions related to pattern separation (Clelland et al., 2009; Sahay et al., 2011; Gu et al., 2012; Kheirbek et al., 2012; Dieni et al., 2016; Lodge and Bischofberger, 2019; Miller and Sahay, 2019). Here we investigated two long-standing hypotheses about the role of inhibition and intrinsic excitability in critical period plasticity. Our results highlight the effectiveness of GABAergic inhibition in suppressing LTP both during and after the critical period and additionally reveal the essential role of T-type Ca^{2+} channels in mediating critical period plasticity by enabling abGCs to overcome that inhibition.

Prior to the critical period, newborn abGCs (<4w) are thought to minimally contribute to information processing due to limited integration into the hippocampal circuit (Esposito et al., 2005; Gu et al., 2012; but see Heigele et al., 2016). Although newborn abGCs exhibit synaptic plasticity in the form of synapse unsilencing facilitated by GABAergic depolarization, plasticity may be most relevant for circuit integration (Chancey et al., 2013; Alvarez et al., 2016), rather than dentate-specific behaviors (Gu et al., 2012). Supporting this idea, in the absence of GABAergic depolarization, abGCs (<4w) exhibit plasticity similar to mature GCs (Ge et al., 2007). By a month after cell birth, the equilibrium potential of chloride reaches mature values (Ge et al., 2006). This switch is followed by the transient 2 week period of enhanced plasticity (4–6 weeks) that corresponds to a time period often used to experimentally assess how selective manipulation affects hippocampal behaviors (Ge et al., 2007; Gu et al., 2012; Miller and Sahay, 2019; Lods et al., 2022).

GABAergic inhibition of mature neurons is well known to limit plasticity by suppressing NMDAR-mediated Ca^{2+} influx (Lovett-Barron et al., 2012; Royer et al., 2012). Compared with mature GCs, abGCs have smaller IPSCs that lead to a lower inhibition–excitation ratio (Marin-Burgin et al., 2012; Dieni et al., 2013; Groisman et al., 2020), reinforcing the possibility that critical period plasticity results from relatively less $GABA_A$ receptor-mediated inhibition. This idea was originally supported by field potential recordings showing that ACSF-LTP requires young

abGCs (Snyder et al., 2001; Saxe et al., 2006; Massa et al., 2011), consistent with our single-cell results showing only 4w–6w abGCs exhibit LTP with inhibition intact. Full innervation from PVs and SSTs also correlates with the closure of the critical period (Groisman et al., 2020), suggestive of a causal role similar to cortical plasticity in the developing visual system (Fagiolini and Hensch, 2000). However, we found that GBZ suppresses dendritic depolarization and LTP to a similar extent in 4w and mature GCs. Suppression of GABA release from PV and nNos-expressing interneurons also robustly increased LTP in 4w abGCs, further showing that plasticity during the critical period is strongly suppressed by synaptic inhibition. Despite incomplete inhibitory innervation, we speculate that feedforward inhibition from dendritic-projecting interneurons like neuroglia-form cells effectively attenuates NMDAR activation via α5 subunit-containing outwardly rectifying $GABA_A$ receptors (Markwardt et al., 2011; Schulz et al., 2018; Vaden et al., 2020; Lodge et al., 2021). But since we enforced spiking via current injections in the TBS induction paradigm, it is possible that minimal somatic inhibition contributes to plasticity via controlling spike generation under more physiological conditions. Nonetheless, our results are consistent with a recent model that poses the switch in GABA polarity from excitatory to inhibitory alters synaptic plasticity from cooperative to competitive, with inhibition during the competitive phase helping abGCs respond to novel aspects that differ between similar input patterns (Gozel and Gerstner, 2021). Our results suggest T-type Ca^{2+} channels boost intrinsic excitability to provide abGCs with a competitive advantage for plasticity. In the absence of both inhibition and T-type Ca^{2+} channel activity, LTP is similar in mature and 4w abGCs (Fig. 6B), potentially implying that the underlying mechanisms of plasticity are otherwise similar.

We were surprised by the ease of LTP induction in mature GCs using whole-cell recording (Fig. 7), in contrast to the lack of LTP using perforated patch with the same TBS (Fig. 2). Our whole-cell results showing a contribution of T-type Ca^{2+} channels to TBS-induced LTP in mature GCs is consistent with previous whole-cell recordings that correlate spike bursts or dendritic sodium spikes with LTP in disinhibited rat slices (Kim et al., 2018, 2023). The whole-cell configuration lowers the access component of series resistance in comparison with perforated patch, potentially allowing greater dendritic depolarization in response to current injections to promote recruitment of voltage-gated channels. Thus, differences in the magnitude of

dendritic depolarization, as well as disruption of endogenous intracellular components (see below), could contribute to different outcomes in whole-cell versus perforated patch recordings. While further studies will be needed to fully elucidate the underlying differences, altogether the results highlight the role of intrinsic excitability and recording mode in setting the threshold for LTP induction.

The differential sensitivity of young and mature GCs to T-type Ca^{2+} channel block in perforated patch recordings cannot be explained by an absence of channel expression in older GCs, as electrophysiological recordings, immunofluorescence, and transcriptomic analysis all indicate the presence of T-type Ca^{2+} channels in mature GCs (Beck et al., 1998; McKay et al., 2006; Dumenieu et al., 2018; Hochgerner et al., 2018). Consistent with the finding that intracellular regulation by G-protein signaling selectively suppresses excitability of mature GCs (Gonzalez et al., 2018), whole-cell recordings that minimize inhibitory G-protein signaling in mature GCs unmasked a contribution of T-type Ca^{2+} channels to intrinsic excitability and LTP. In contrast, with an intact intracellular milieu provided by perforated patch, T-type Ca^{2+} channel activity was readily apparent in young but not mature GCs (Figs. 4, 6). T-type Ca^{2+} channels in mature GCs may be under direct suppression by G-protein signaling, or the contribution of T-type Ca^{2+} channels to intrinsic excitability may be masked by activation or regulation of other ion channels, like GIRKs or NALCN (Gonzalez et al., 2018, 2023). The density or location of T-type Ca^{2+} channels may also change across GC maturation, and increasing voltage-gated K^+ conductances might effectively counteract T-type Ca^{2+} channel activation (Mongiat et al., 2009). Importantly, intrinsic excitability of mature GCs is dynamic, changing in response to experience and time of day, potentially contributing to heterogeneity in the propensity for plasticity (Pignatelli et al., 2019; Gonzalez et al., 2023; Kim et al., 2023). Future studies will be needed to fully dissect the mechanisms underlying the role of T-type Ca^{2+} channels in critical period plasticity and the changes in intrinsic excitability that contribute to closure of the critical period. In young GCs, depolarization provided by T-type Ca^{2+} channels clearly contributes to voltage-dependent magnesium unblock of NMDARs (Fig. 5), although Ca^{2+} influx via T-type channels could also serve as a signaling molecule in young GCs with a low buffer capacity to spatially restrict free Ca^{2+} (Stocca et al., 2008). Together, our results support the long-standing idea that intrinsic excitability conferred by T-type Ca^{2+} channel activity in young abGCs underlies a low threshold for plasticity (Schmidt-Hieber et al., 2004) and further reveals the potential capacity for T-type Ca^{2+} channels to promote plasticity in mature GCs.

References

Abrahamsson T, Cathala L, Matsui K, Shigemoto R, Digregorio DA (2012) Thin dendrites of cerebellar interneurons confer sublinear synaptic integration and a gradient of short-term plasticity. Neuron 73:1159–1172.

Alvarez DD, Giacomini D, Yang SM, Trinchero MF, Temprana SG, Buttner KA, Beltramone N, Schinder AF (2016) A disynaptic feedback network activated by experience promotes the integration of new granule cells. Science 354:459–465.

Beck H, Steffens R, Elger CE, Heinemann U (1998) Voltage-dependent Ca2+ currents in epilepsy. Epilepsy Res 32:321–332.

Bischofberger J, Engel D, Li L, Geiger JR, Jonas P (2006) Patch-clamp recording from mossy fiber terminals in hippocampal slices. Nat Protoc 1:2075–2081.

Chancey J, Adlaf E, Sapp M, Pugh P, Wadiche J, Overstreet-Wadiche L (2013) GABA depolarization is required for experience-dependent synapse unsilencing in adult-born neurons. J Neurosci 33:6614–6622.

Clelland C, et al. (2009) A functional role for adult hippocampal neurogenesis in spatial pattern separation. Science 325:210–213.

Cushman JD, Drew MR, Krasne FB (2021) The environmental sculpting hypothesis of juvenile and adult hippocampal neurogenesis. Prog Neurobiol 199:101961.

Deng W, Saxe MD, Gallina IS, Gage FH (2009) Adult-born hippocampal dentate granule cells undergoing maturation modulate learning and memory in the brain. J Neurosci 29:13532–13542.

Dieni CV, Nietz AK, Panichi R, Wadiche JI, Overstreet-Wadiche L (2013) Distinct determinants of sparse activation during granule cell maturation. J Neurosci 33:19131–19142.

Dieni CV, Panichi R, Aimone JB, Kuo CT, Wadiche JI, Overstreet-Wadiche L (2016) Low excitatory innervation balances high intrinsic excitability of immature dentate neurons. Nat Commun 7:11313.

Dreyfus FM, Tscherter A, Errington AC, Renger JJ, Shin HS, Uebele VN, Crunelli V, Lambert RC, Leresche N (2010) Selective T-type calcium channel block in thalamic neurons reveals channel redundancy and physiological impact of I(T)window. J Neurosci 30:99–109.

Dumenieu M, Senkov O, Mironov A, Bourinet E, Kreutz MR, Dityatev A, Heine M, Bikbaev A, Lopez-Rojas J (2018) The low-threshold calcium channel Cav3.2 mediates burst firing of mature dentate granule cells. Cereb Cortex 28:2594–2609.

Esposito M, Piatti V, Laplagne D, Morgenstern N, Ferrari C, Pitossi F, Schinder A (2005) Neuronal differentiation in the adult hippocampus recapitulates embryonic development. J Neurosci 25:10074–10086.

Fagiolini M, Hensch TK (2000) Inhibitory threshold for critical-period activation in primary visual cortex. Nature 404:183–186.

Ge S, Goh E, Sailor K, Kitabatake Y, Ming G, Song H (2006) GABA regulates synaptic integration of newly generated neurons in the adult brain. Nature 439:589–593.

Ge S, Yang C, Hsu K, Ming G, Song H (2007) A critical period for enhanced synaptic plasticity in newly generated neurons of the adult brain. Neuron 54:559–566.

Glickfeld LL, Atallah BV, Scanziani M (2008) Complementary modulation of somatic inhibition by opioids and cannabinoids. J Neurosci 28:1824–1832.

Goncalves JT, Bloyd CW, Shtrahman M, Johnston ST, Schafer ST, Parylak SL, Tran T, Chang T, Gage FH (2016) In vivo imaging of dendritic pruning in dentate granule cells. Nat Neurosci 19:788–791.

Gonzalez JC, Epps SA, Markwardt SJ, Wadiche JI, Overstreet-Wadiche L (2018) Constitutive and synaptic activation of GIRK channels differentiates mature and newborn dentate granule cells. J Neurosci 38:6513–6526.

Gonzalez JC, Lee H, Vincent AM, Hill AL, Goode LK, King GD, Gamble KL, Wadiche JI, Overstreet-Wadiche L (2023) Circadian regulation of dentate gyrus excitability mediated by G-protein signaling. Cell Rep 42:112039.

Gozel O, Gerstner W (2021) A functional model of adult dentate gyrus neurogenesis. Elife 10:e66463.

Groisman AI, Yang SM, Schneider AF (2020) Differential coupling of adult-born granule cells to parvalbumin and somatostatin interneurons. Cell Rep 30:202–214.

Gu Y, Arruda-Carvalho M, Wang J, Janoschka S, Josselyn S, Frankland P, Ge S (2012) Optical controlling reveals time-dependent roles for adult-born dentate granule cells. Nat Neurosci 15:1700–1706.

Heigele S, Sultan S, Toni N, Bischofberger J (2016) Bidirectional GABAergic control of action potential firing in newborn hippocampal granule cells. Nat Neurosci 19:263–270.

Hochgerner H, Zeisel A, Lönnerberg P, Linnarsson S (2018) Conserved properties of dentate gyrus neurogenesis across postnatal development revealed by single-cell RNA sequencing. Nat Neurosci 21:290–299.

Kheirbek MA, Tannenholz L, Hen R (2012) NR2B-dependent plasticity of adult-born granule cells is necessary for context discrimination. J Neurosci 32:8696–8702.

Kim Y, Kim S, Ho WK, Lee SH (2023) Burst firing is required for induction of Hebbian LTP at lateral perforant path to hippocampal granule cell synapses. Mol Brain 16:45.

Kim S, Kim Y, Lee SH, Ho WK (2018) Dendritic spikes in hippocampal granule cells are necessary for long-term potentiation at the perforant path synapse. Elife 7:e35269.

Krook-Magnuson E, Luu L, Lee S, Varga C, Soltesz I (2011) Ivy and neurogliaform interneurons are a major target of mu-opioid receptor modulation. J Neurosci 31:14861–14870.

Larimer P, Strowbridge B (2010) Representing information in cell assemblies: persistent activity mediated by semilunar granule cells. Nat Neurosci 13:213–222.

Li Y, Aimone J, Xu X, Callaway E, Gage F (2012) Development of GABAergic inputs controls the contribution of maturing neurons to the adult hippocampal network. Proc Natl Acad Sci U S A 109:4290–4295.

Li L, Sultan S, Heigele S, Schmidt-Salzmann C, Toni N, Bischofberger J (2017) Silent synapses generate sparse and orthogonal action potential firing in adult-born hippocampal granule cells. Elife 6:e23612.

Lodge M, Bischofberger J (2019) Synaptic properties of newly generated granule cells support sparse coding in the adult hippocampus. Behav Brain Res 372:112036.

Lodge M, Hernandez MC, Schulz JM, Bischofberger J (2021) Sparsification of AP firing in adult-born hippocampal granule cells via voltage-dependent alpha5-GABA(A) receptors. Cell Rep 37:109768.

Lods M, et al. (2022) Chemogenetic stimulation of adult neurogenesis, and not neonatal neurogenesis, is sufficient to improve long-term memory accuracy. Prog Neurobiol 219:102364.

Lopez-Rojas J, Heine M, Kreutz MR (2016) Plasticity of intrinsic excitability in mature granule cells of the dentate gyrus. Sci Rep 6:21615.

Lovett-Barron M, Turi G, Kaifosh P, Lee P, Bolze F, Sun X, Nicoud J, Zemelman B, Sternson S, Losonczy A (2012) Regulation of neuronal input transformations by tunable dendritic inhibition. Nat Neurosci 15:423–430, S421–423.

Marin-Burgin A, Mongiat L, Pardi M, Schinder A (2012) Unique processing during a period of high excitation/inhibition balance in adult-born neurons. Science 335:1238–1242.

Markwardt S, Dieni C, Wadiche J, Overstreet-Wadiche L (2011) Ivy/neurogliaform interneurons coordinate activity in the neurogenic niche. Nat Neurosci 14:1407–1409.

Martinello K, Huang Z, Lujan R, Tran B, Watanabe M, Cooper EC, Brown DA, Shah MM (2015) Cholinergic afferent stimulation induces axonal function plasticity in adult hippocampal granule cells. Neuron 85:346–363.

Massa F, Koehl M, Wiesner T, Grosjean N, Revest JM, Piazza PV, Abrous DN, Oliet SH (2011) Conditional reduction of adult neurogenesis impairs bidirectional hippocampal synaptic plasticity. Proc Natl Acad Sci U S A 108:6644–6649.

McKay BE, McRory JE, Molineux ML, Hamid J, Snutch TP, Zamponi GW, Turner RW (2006) Ca(V)3 T-type calcium channel isoforms differentially distribute to somatic and dendritic compartments in rat central neurons. Eur J Neurosci 24:2581–2594.

Miller SM, Sahay A (2019) Functions of adult-born neurons in hippocampal memory interference and indexing. Nat Neurosci 22:1565–1575.

Mishra P, Narayanan R (2022) Conjunctive changes in multiple ion channels mediate activity-dependent intrinsic plasticity in hippocampal granule cells. iScience 25:103922.

Mongiat L, Esposito M, Lombardi G, Schinder A (2009) Reliable activation of immature neurons in the adult hippocampus. PLoS One 4:e5320.

Mongiat L, Schinder A (2011) Adult neurogenesis and the plasticity of the dentate gyrus network. Eur J Neurosci 33:1055–1061.

Nakashiba T, et al. (2012) Young dentate granule cells mediate pattern separation, whereas old granule cells facilitate pattern completion. Cell 149:188–201.

Overstreet-Wadiche L, Bensen A, Westbrook G (2006) Delayed development of adult-generated granule cells in dentate gyrus. J Neurosci 26:2326–2334.

Piatti V, Davies-Sala M, Esposito M, Mongiat L, Trinchero M, Schinder A (2011) The timing for neuronal maturation in the adult hippocampus is modulated by local network activity. J Neurosci 31:7715–7728.

Pignatelli M, Ryan TJ, Roy DS, Lovett C, Smith LM, Muralidhar S, Tonegawa S (2019) Engram cell excitability state determines the efficacy of memory retrieval. Neuron 101:274–284.e5.

Remmers CL, Castillon CCM, Armstrong JN, Contractor A (2020) Recruitment of parvalbumin and somatostatin interneuron inputs to adult born dentate granule neurons. Sci Rep 10:17522.

Royer S, Zemelman B, Losonczy A, Kim J, Chance F, Magee J, Buzsaki G (2012) Control of timing, rate and bursts of hippocampal place cells by dendritic and somatic inhibition. Nat Neurosci 15:769–775.

Sahay A, Scobie K, Hill A, O'Carroll C, Kheirbek M, Burghardt N, Fenton A, Dranovsky A, Hen R (2011) Increasing adult hippocampal neurogenesis is sufficient to improve pattern separation. Nature 472:466–470.

Saxe M, et al. (2006) Ablation of hippocampal neurogenesis impairs contextual fear conditioning and synaptic plasticity in the dentate gyrus. Proc Natl Acad Sci U S A 103:17501–17506.

Schinder AF, Gage FH (2004) A hypothesis about the role of adult neurogenesis in hippocampal function. Physiology 19:253–261.

Schmidt-Hieber C, Jonas P, Bischofberger J (2004) Enhanced synaptic plasticity in newly generated granule cells of the adult hippocampus. Nature 429:184–187.

Schmidt-Salzmann C, Li L, Bischofberger J (2014) Functional properties of extrasynaptic AMPA and NMDA receptors during postnatal hippocampal neurogenesis. J Physiol 592:125–140.

Schulz JM, Knoflach F, Hernandez MC, Bischofberger J (2018) Dendrite-targeting interneurons control synaptic NMDA-receptor activation via nonlinear alpha5-GABA(A) receptors. Nat Commun 9:3576.

Skaggs WE, McNaughton BL, Wilson MA, Barnes CA (1996) Theta phase precession in hippocampal neuronal populations and the compression of temporal sequences. Hippocampus 6:149–172.

Snyder J, Kee N, Wojtowicz J (2001) Effects of adult neurogenesis on synaptic plasticity in the rat dentate gyrus. J Neurophysiol 85:2423–2431.

Stocca G, Schmidt-Hieber C, Bischofberger J (2008) Differential dendritic Ca2+ signalling in young and mature hippocampal granule cells. J Physiol 586:3795–3811.

Sun GJ, Sailor KA, Mahmood QA, Chavali N, Christian KM, Song H, Ming GL (2013) Seamless reconstruction of intact adult-born neurons by serial end-block imaging reveals complex axonal guidance and development in the adult hippocampus. J Neurosci 33:11400–11411.

Taniguchi H, et al. (2011) A resource of Cre driver lines for genetic targeting of GABAergic neurons in cerebral cortex. Neuron 71:995–1013.

Temprana SG, Mongiat LA, Yang SM, Trinchero MF, Alvarez DD, Kropff E, Giacomini D, Beltramone N, Lanuza GM, Schinder AF (2015) Delayed coupling to feedback inhibition during a critical period for the integration of adult-born granule cells. Neuron 85:116–130.

Tovar K, Westbrook G (1999) The incorporation of NMDA receptors with a distinct subunit composition at nascent hippocampal synapses in vitro. J Neurosci 19:4180–4188.

Vaden RJ, Gonzalez JC, Tsai MC, Niver SJ, Fullister A, Griffith C, Kramer R, Wadiche J, Overstreet-Wadiche L (2020) Parvalbumin interneurons provide spillover to newborn and mature dentate granule cells. Elife 9:e54125.

Vyleta NP, Snyder JS (2021) Prolonged development of long-term potentiation at lateral entorhinal cortex synapses onto adult-born neurons. PLoS One 16:e0253642.

Wang W, et al. (2016) A primary cortical input to hippocampus expresses a pathway-specific and endocannabinoid-dependent form of long-term potentiation. eNeuro 3:4.

Wang S, Scott B, Wojtowicz J (2000) Heterogenous properties of dentate granule neurons in the adult rat. J Neurobiol 42:248–257.

Yang SM, Alvarez DD, Schneider AF (2015) Reliable genetic labeling of adult-born dentate granule cells using ascl1CreERT2 and glastCreERT2 murine lines. J Neurosci 35:15379–15390.